第32卷 第8期 焊 接 学 报 Vol. 32 No. 8
2011年8月 TRANSACTIONS OF THE CHINA WELDING INSTITUTION August 2011

62Sn36Pb2Ag钎料中Ag元素对AgCu/SnPbAg/CuBe焊缝性能的影响

丁 颖[1], 申 坤[1], 张 冉[2]
(1. 北京控制工程研究所, 北京 100190; 2. 北京工业大学 机械工程与应用电子学院, 北京 100124)

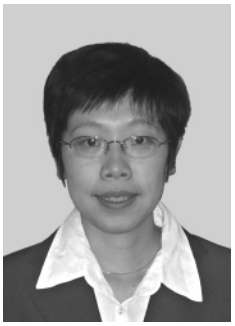

丁 颖

摘 要: 分别采用62Sn36Pb2Ag钎料和63Sn37Pb共晶钎料焊接AgCu合金块和CuBe合金片进行试验,对比分析两种钎料形成的焊缝性能和显微组织结构,阐述了62Sn36Pb2Ag钎料中Ag元素的存在对AgCu/SnPbAg/CuBe焊缝性能的影响机制. 结果表明,62Sn36Pb2Ag钎料中的Ag元素对于润湿铺展状态的改变有利于控制焊缝内部气孔含量,弥散分布于焊缝内部的Ag_3Sn颗粒状结构能够有效钉扎位错而提高焊缝强度,钎焊温度下银含量接近饱和的状态有效抑制了界面附近脆性Ag_3Sn相的局部富集,优化了焊缝显微组织.

关键词: 锡铅银钎料; 银基合金; 钎焊
中图分类号: TG115.28 **文献标识码:** A **文章编号:** 0253-360X(2011)08-0065-04

0 序 言

电子互联中铜的钎焊连接,最常用的是63Sn37Pb钎料[1],锡与铜反应,界面生成Sn-Cu金属间化合物(intermetallic compound,IMC),完成良好的冶金结合. 但如果银的钎焊也采用63Sn37Pb钎料,则会产生"银蚀"和危险脆性相的问题. 对于纯银,由于银在熔融SnPb钎料中的溶解速度要比铜快很多,银层过薄,会造成银层脱蚀,严重弱化结合强度,即为所谓的"银蚀"现象[2]. 另外,锡与银反应,生成金属间化合物Ag_3Sn. Ag_3Sn是一种脆性相,如果过多的Ag元素融入钎料并局部富集,界面附近生成针状、棒状、甚至块状的Ag_3Sn,具有这样脆性相形态的Ag_3Sn,将对焊点的服役性能造成不良影响[3].

ECSS-Q-ST-70-08A《高可靠电连接的手工焊接》中关于钎料类型的选择指南[2]中指出: 对于具有银焊盘或银镀层的元器件钎焊,应选用62Sn36Pb2Ag钎料,原因是这种钎料内部的银成分已几近饱和,可防止焊盘处的银从表面脱蚀. 对于薄膜含银镀层的钎焊,早期文献[4,5]报道中已经表明,采用SnPbAg钎料代替SnPb共晶钎料,能够解决一系列可靠性隐患问题. 但对于这一过程中,Ag_3Sn脆性相的生成形态及其对焊点的影响却没有提及. 另外,对于结构件中涉及较厚银层的钎焊,SnPbAg钎料是否能够合理取代SnPb共晶钎料,未见相关报道. 文中针对这一问题,采用63Sn37Pb和62Sn36Pb2Ag钎料焊接AgCu合金块与CuBe合金片,对焊缝性能,包括焊缝力学性能和显微组织结构,进行了对比分析和研究,阐明了62Sn36Pb2Ag钎料中Ag元素的存在对焊缝性能的影响机制.

1 试验方法

钎焊样件结构组成如图1所示,合金片材料是铍青铜,即含少量铍的CuBe合金,表面镀Ni/Au保护,尺寸为5 mm×30 mm×0.5 mm,铜片背面有两个直径1.5 mm的出气和观察孔; 合金块材料是银铜合金,化学成分(质量分数,%)为(95~98)Ag(2~5)Cu,尺寸为3 mm×9 mm×3 mm. 二者之间的钎焊,通过手工操纵智能电烙铁,熔化助焊剂含量为2.1%的焊锡丝完成,钎料选用63Sn37Pb和62Sn36Pb2Ag. 焊缝两侧连接面积为合金块的表面积. 试验包括手工焊接样件、力学性能测试和显微组织分析三个环节.

手工焊接样件的具体操作过程如下: (1) 焊前样件清洗. (2) 搪锡,将合金片待焊一面去金处理; 将合金块待焊一侧表面搪锡,熔化直径1.0 mm的

收稿日期: 2010-06-22
基金项目: 航天科技集团公司重大工艺基金资助项目(ZDGY2010-14)

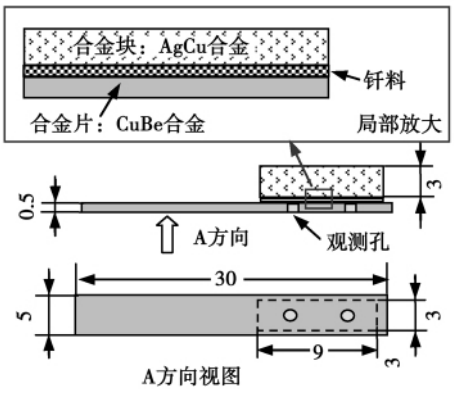

图 1 Ag/Cu 连接试验样件结构示意图 (mm)

Fig. 1 Structure schematics of Ag/Cu connection specimen

锡丝长度 12 mm. (3) 钎焊: 用工装固定合金块,用镊子将合金片压在搪好锡的合金块上,用电烙铁加热合金片背面,使先搪的锡熔化成一体,并在合金片的两个通气孔冒出锡珠. 此时,用工装压住合金片背面,移走烙铁,待焊锡冷却后再将工装抬起,完成焊接. (4) 焊后清洗,去掉助焊剂残渣. 试验共制样 20 件,其中 63Sn37Pb 钎料的焊缝样件 10 件,62Sn36Pb2Ag 钎料的焊缝样件 10 件.

力学性能测试主要是对样件进行侧向剪切力拉伸试验. 试验利用 Instron 电子万能材料试验机,采用控制位移的方法,对样品进行剪切测试. 制作合适的剪切工装,一侧夹具夹紧合金块,另一侧夹具夹紧合金片,进行拉伸并记录试验数据. 根据钎料合金的力学性能,位移速率定为 5 mm/min,以忽略蠕变行为的影响[6]. 剪切测试中,每种钎料的焊接样件各测试 5 件,以便统计分析数据.

用于金相观察的样品制作,先用树脂塑封,再对合金块长度方向的焊缝进行打磨剖光,每种钎料样件各剖分 5 件. 试验采用光学显微镜进行低倍观察,对局部位置,特别是钎料与 AgCu 合金块母材的界面区域,进行扫描电镜(scanning electron microscopy,SEM)观察和成分分析.

2 试验结果及讨论

2.1 力学性能测试

两种钎料的焊缝剪切力测试结果如表 1 所示. 其中,63Sn37Pb 钎料焊缝的破坏形式多为 A 型,62Sn36Pb2Ag 钎料焊缝的破坏形式全部为 B 型,具体见图 2. A 型破坏指的是断面布满整个焊缝,合金块与合金片完全剪切分离,所测力值为焊缝的真实剪切力值; 而 B 型破坏指的是断面位于合金片观察孔处,所测力值约为 1/4 焊缝剪切力加上有小孔的合金片截面抗拉力,该数据小于真实剪切力值.

表 1 两种钎料焊接的焊缝剪切力测试结果

Table 1 Results of solder joint shear test for two kinds of solder alloys

焊缝内钎料	序号	测出最大剪切力值 F_1/N	破坏形式	焊缝真实剪切力值 F_2/N	测试平均剪切力值 F_3/N
63Sn37Pb	1	512.3	A	512.3	
	2	569.2	A	569.2	
	3	735.3	B	>735.3	616.9
	4	664.1	A	664.1	
	5	603.8	A	603.8	
62Sn36Pb2Ag	1	846.7	B	>846.7	
	2	833.1	B	>833.1	
	3	812.8	B	>812.8	846.4
	4	847.9	B	>847.9	
	5	891.3	B	>891.3	

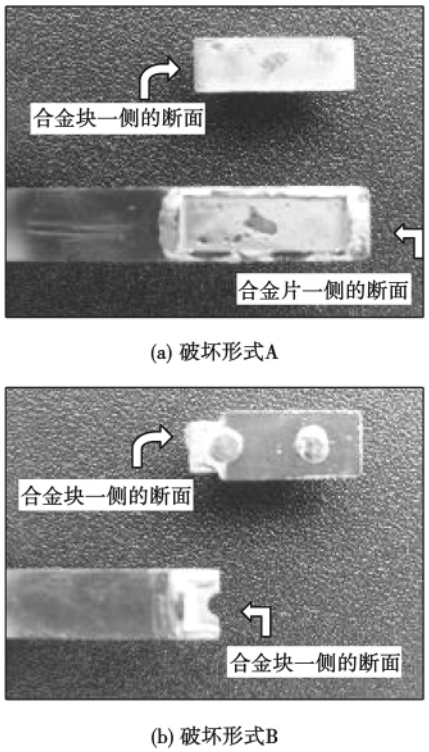

图 2 焊缝样件剪切力测试后的两种破坏形式

Fig. 2 Two failure modes for solder joints after shear test

结果表明,62Sn36Pb2Ag 钎料的焊缝结合力要明显高于 63Sn37Pb 钎料. 这是因为在 62Sn36Pb2Ag 钎料中的 Ag 元素,会以 Ag_3Sn 的形式呈颗粒状分布,在材料受力变形过程中,起到了位错钉扎的作用[7],阻碍位错的运动,提高了材料的强度,表现为焊缝剪应力值升高.

由此可见,从力学性能角度讲,62Sn36Pb2Ag 钎

料的焊缝性能要优于 63Sn37Pb 钎料.

2.2　金相观察与分析

2.2.1　气孔的生成

63Sn37Pb 共晶钎料的熔点为 183 ℃,而 62Sn36Pb2Ag 并非共晶钎料,存在熔化区间,其固相点为 175 ℃,液相点为 189 ℃. 从焊接可操作性来看,二者无明显差别. 但是,其内部生成的气孔情况有所不同. 表 2 是两种钎料形成的焊缝样件剖分后,经过 50 倍下的光学显微镜统计出来的孔洞长度占焊缝总长度的比例情况.

表 2　两种钎料焊接的焊缝内部气孔生成比例(%)

Table 2　Void percentage inside solder joint for two kinds of solder alloys

序号	63Sn37Pb 焊缝气孔比例	62Sn36Pb2Ag 焊缝气孔比例
1	21	0.2
2	15	1
3	23	5
4	12	3
5	8	0.8

不难看出,62Sn36Pb2Ag 钎料形成的焊缝,内部气孔生成率低,焊缝内部钎料填充率高; 而 63Sn37Pb 钎料形成的焊缝,内部存在一定程度的气孔. 由于结构样件尺寸相对电子元器件要大很多,特别是合金块热容较大,搪锡过程中,63Sn37Pb 钎料熔化后在合金块表面润湿铺展,很快就冷却凝固,在较大体积的钎料内部,助焊剂挥发所产生的气体不能完全及时地排出,气孔在内部形成. 尽管在随后的合金片焊接过程中,有两个观察孔可以用作出气孔,但仍无法充分释放在搪锡过程中就形成的气泡. 然而,62Sn36Pb2Ag 钎料由于含有质量分数 2% 的银,具有一定的熔化范围,凝固速度较 63Sn37Pb 共晶钎料有所延迟,润湿铺展行为也不尽相同,有可能在润湿冷凝过程中,可以更为有效地排放气体.

2.2.2　显微组织分析

图 3 是两种钎料形成的焊缝剖分后,在光学显微镜焊缝附近的显微组织形貌. 可见,两种钎料都与母材发生反应,界面生成了 IMC,与 AgCu 合金块的界面生成了 Ag_3Sn IMC 层,与 CuBe 合金片的界面生成了 Cu6Sn5 IMC 层. 但不同的是,63Sn37Pb 钎料焊缝内部,由于合金块中的 Ag 元素向熔融 Sn-Pb 钎料中的快速溶解和局部富集,生成了灰色的大块 Ag_3Sn 脆性相,显微组织由 Sn-Pb 共晶组织和棒状或块状 Ag_3Sn 构成; 而 62Sn36Pb2Ag 钎料的焊缝内部,因为质量分数 2% 银含量的存在,在熔化温度下银成分已接近饱和,合金块中的 Ag 元素向熔融钎料中的扩散受到限制,没有局部富集而析出过量的块状 Ag_3Sn,显微组织由钎料本身生成的颗粒状 Ag_3Sn 和 Sn-Pb 固溶体构成.

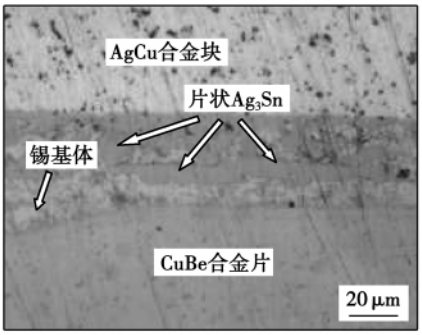

(a) 63Sn37Pb钎料形成的焊缝显微组织形貌

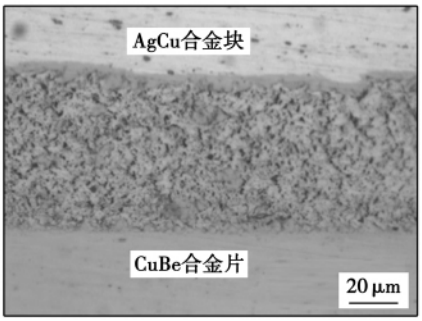

(b) 62Sn36Pb2Ag钎料形成的焊缝显微组织形貌

图 3　两种钎料形成的焊缝内部脆性相生成情况

Fig. 3　Brittle phase formation inside solder joints for two kinds of solder alloys

据文献[3]记载,适当的 IMC 层对于焊料和母材之间形成良好的冶金结合是必要的,但当 IMC 层过厚或有致命脆性相生成时[3](例如 $AuSn_4$),低载荷下容易造成机械损伤. 此外,焊点中的 IMC 在后期服役过程中由于受热还会继续长大,当 IMC 生长超过安全厚度或长大的脆性相成为焊点内的应力集中点时,就会引发焊点的可靠性危机.

对于脆性相 Ag_3Sn,如果 Ag_3Sn 的形态趋向于针状、棒状或片状时,它对焊点性能将产生负面影响. 当受外力作用时,这种棒状 Ag_3Sn 很难与富锡基体协调一致地变形,二者较大的抗变形能力差异将导致裂纹沿 Ag_3Sn 与富锡基体的界面萌生并扩展,最终造成焊点失效. 因此,应当合理避免具有危险形态的脆性相生成. 62Sn36Pb2Ag 钎料中 Ag 元素的存在由于抑制了母材银成分的溶解,而控制了界面附近 Ag_3Sn 脆性相的局部富集长大. 内部 Ag 元素在钎料熔化过程中以颗粒状 Ag_3Sn 的形态弥散分布于焊点组织内部,如图 4 所示. 表 3 为图 4 的

62Sn36Pb2Ag 钎料中 Ag_3Sn 颗粒的能谱确定，它可以有效起到钉扎位错的作用，提高了焊点强度.

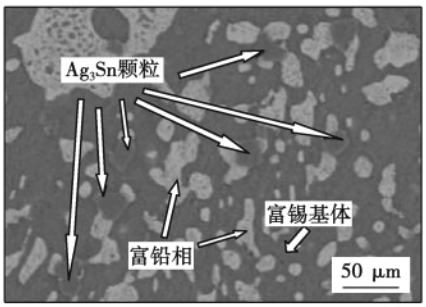

图 4 62Sn36Pb2Ag 钎料形成焊缝的内部显微组织及 Ag_3Sn 颗粒能谱确定

Fig. 4 Microstructure inside 62Sn36Pb2Ag solder joint

表 3 62Sn36Pb2Ag 钎料中 Ag_3Sn 颗粒能谱确定

Table 3 EDX identification of Ag_3Sn particles in 62Sn36Pb2Ag solder

元素	质量分数(%)	原子分数(%)
Ag	73.09	74.93
Sn	26.91	25.07

3 结 论

(1) 两种钎料的可焊性相当，但 62Sn36Pb2Ag 钎料形成的焊缝内部气孔含量少，焊接工艺性优于 63Sn37Pb 钎料.

(2) 62Sn36Pb2Ag 钎料内部颗粒状 Ag_3Sn，能够有效钉扎位错，其焊缝剪切力高于 63Sn37Pb 钎料，焊缝的力学性能优于 63Sn37Pb 钎料.

(3) 62Sn36Pb2Ag 钎料内部 Ag 元素的存在抑制了母材 Ag 元素的扩散和富集，块状形态的 Ag_3Sn 脆性相没有出现在其显微组织中，有效控制了脆性焊点的形成，焊缝的可靠性优于 63Sn37Pb 钎料.

(4) 62Sn36Pb2Ag 钎料中的 Ag 元素对优化 AgCu/钎料/CuBe 焊缝的焊接工艺性、减少气孔含量、增强焊缝结合力，以及提高焊缝可靠性都有着至关重要的作用，建议采用此种钎料焊接银基合金.

参考文献:

[1] Ahat Shawkret, Du Liguang. Effect of aging on the microstructure and shear strength of SnPbAg/Ni-P/Cu and SnAg/Ni-P/Cu solder joints [J], Journal of Electronic Materials, 2000, 29(9): 1105 - 1109.

[2] European Cooperation for Space Standardization. The manual soldering of high-reliability electrical connections [M]. ECSS-Q-ST-70-08A, 1999.

[3] Zeng K, Tu K N. Six cases of reliability study of Pb-free solder joints in electronic packaging technology [J]. Materials Science and Engineering R, 2002, 38: 55 - 105.

[4] Chiou Bishiou, Liu K C. Intermetallic formation on the fracture of Sn/Pb solder and Pd/Ag conductor interfaces [J]. IEEE Transactions on CHMT, 1990, 13(2): 267 - 274.

[5] Li G Y, Chan Y C. Aging effects on shear fatigue life of solder joint between Pd/Ag conductor and Sn/Pb/Ag solder [C] // IEEE CPMT Electronic Packaging Technology Conference, 1997: 102 - 107.

[6] Ding Y, Wang C Q. Aging effects on fracture behavior of 63Sn37Pb eutectic solder during tensile tests under the SEM [J]. Materials Science and Engineering A, 2004, 384(10): 314 - 323.

[7] Kerr M, Chawla N. Creep deformation behavior of Sn-3.5Ag solder/Cu couple at small length scales [J]. Acta Materialia, 2004, 52: 4527 - 4535.

[8] Chan Y C, So Alex C K. Growth kinetic studies of Cu-Sn intermetallic compound and its effect on shear strength of LCCC SMT solder joints [J]. Materials Science & Engineering B, 1998, 55: 5 - 13.

作者简介: 丁 颖，女，1978 年出生，博士，高级工程师. 长期从事微电子封装与组装研究. 现已发表论文 20 余篇. Email: dingyzoe@gmail.com

通讯作者: 申 坤，女，硕士，高级工程师. Email: shenkun_2005@sohu.com

improved. The best wettability and mechanical property of soldered joint is obtained when the content of Pr is 0.05 wt. %. Moreover, when the content of Pr is exceeded 0.1 wt. %, plenty of Sn-Pr compounds are found in the Sn-9Zn solder, which lead to the growth of whiskers.

Key words: rare earth Pr; wettability; microstructure; mechanical property; Sn whisker

Characteristics analysis of combined plasma arc based on sequential coupling method of physics environment approach

MENG Jianbing[1], XU Wenji[2], DONG Xiaojuan[1], YIN Zhanmin[1] (1. Shandong Provincial Key Laboratory of Precision Manufacturing and Non-traditional Machining, Shandong University of Technology, Zibo 255049, China; 2. Key Laboratory for Precision and Non-traditional Machining Technology of Ministry of Education, Dalian University of Technology, Dalian 116024, China). p 57 - 60

Abstract: According to the features of combined plasma arc and the theory of magnetic fluid dynamics and electromagnetics, which exists a coexistence of transferred arc and non-transferred arc and an interaction of electric field, magnetic field, thermal field and flow field, a three-dimensional mathematical model was developed. The effects of working current and gas flow on the distribution of jet temperature of the combined plasma arc were analyzed by finite element software ANSYS and sequential coupling method. The results show that the simulation value with this model is consistent with the measured value.

Key words: physics environment; sequential coupling method; combined plasma arc; performance evaluation

Motion control algorithm of cutting robot for ellipsoidal pressure vessels opening

LIU Tao[1], WANG Zongyi[1], DU Hongwang[1], XIE Jujun[2] (1. College of Automation, Harbin Engineering University, Harbin 150001, China; 2. Daqing Oilfield Engineering Co., Ltd., Daqing 163712, China). p 61 - 64

Abstract: According to ellipsoidal pressure vessels opening and cutting groove, a special four degrees of freedom cutting robot was developed. The mechanical structure and the working principle were introduced, and the intersecting line mathematic model of ellipsoidal shells opening in polar coordinates was established by using space analytic geometry. The groove angle calculation formula and four-axis motion control algorithm during groove cutting were derived, and ideal movement trajectory was obtained through linear interpolation algorithm. In order to eliminate the disturbances of location error and vessel distortion, teaching compensation algorithm based on theory calculation was proposed to correct robot motion trajectory. The practical application results illustrated that opening and groove cutting can be realized with the special cutting robot, and the cutting quality meets the technology requirements.

Key words: utting robot; groove cutting; intersecting line calculation; interpolation

Influence of Ag element in 62Sn36Pb2Ag on properties of AgCu/SnPbAg/CuBe solder joint

DING Ying[1], SHEN Kun[1], ZHANG Ran[2] (1. Beijing Institute of Control Engineering, Beijing 100190, China; 2. College of Mechanical Engineering and Applied Electronics Technology, Beijing University of Technology, Beijing 100124, China). p 65 - 68

Abstract: 62Sn36Pb2Ag solder and 63Sn37Pb eutectic solder were adopted to join the AgCu alloy bulk and CuBe alloy sheet. The mechanical properties and the relative microstructure for both solder joints were compared and analyzed by the experimental studies. The influence mechanism of Ag element in 62Sn36Pb2Ag on the properties of the AgCu/SnPbAg/CuBe solder joint was elaborated in detail accordingly. The results show that the Ag element in the solder changes the wetting behavior and benefits the less voids, the dispersed distribution of the Ag_3Sn particles contributes the dislocation clinching and results in the higher solder joint strength, and the nearly saturated state of Ag content in the solder joint under the soldering temperature prevents the brittle Ag3Sn phase enriching near the interface and gives the ideal microstructure of the solder joint.

Key words: 62Sn36Pb2Ag solder; Ag-based alloy; soldering

Analysis of current-carrying region of TIG arc with low-disturbing electrostatic probe

LI Yuanbo, ZHU Liang (State Key Laboratory of Gansu Advanced Non-ferrous Metal Materials, Lanzhou University of Technology, Lanzhou 730050, China). p 69 - 72

Abstract: For understanding the character of TIG arc current-carrying region and ascertaining the range of current-carrying region, a low-disturbing electrostatic probe was developed to measure the potential of probe in floating condition and the current of probe with bias voltage in various sections along the axial direction of arc. The results show that it can get the ion saturated current by probe with negative bias voltage and the electron saturated current by probe with positive bias voltage. And then the half widths of the ion saturated current peak and the electron saturated current peak can represent the radius of current-carrying region and arc including peripheral negative ion region respectively. Both of the range of current-carrying region and arc increase into widest near anode from cathode to anode along the axial direction of arc. In addition, it is found that the effect on probe caused by peripheral negative ion region of arc can reduce the potential of probe in floating condition. This effect can be neglected when the exposed length is decreased into 5 - 6 mm.

Key words: low-disturbing electrostatic probe; current-carrying region; arc; exposed length of probe

Friction stir fillet welding of 2519 aluminum alloys

MA Huikun, HE Diqiu, LIU Jinshu (College of Mechanical and Electrical Engineering, Central South University, Changsha 410083, China). p 73 - 76

Abstract: Using a new method of fillet welding, the friction stir outer fillet welding, we welded the 2519 high-strength aluminum alloy plate 22 mm thick, and analyzed the microstructure and microhardness distribution of fillet welding joint and the reason of the fracture of welding stirring pin, which the type of fracture is shear fracture. The results show that the welding method can effectively carry on fillet welding; the reasonable